Grazing incidence small angle x-ray scattering from free-standing nanostructures

Markus Rauscher,[a] Rogerio Paniago,[b] Hartmut Metzger, Zoltan Kovats, Jan Domke, and Johann Peisl
Sektion Physik der Ludwig-Maximilians Universität München, Geschwister-Scholl-Platz 1, D-80539 München, Germany

Hans-Dieter Pfannes
Departamento de Fisica, Universidade Federal de Minas Gerais, Caixa Postal 702, 30123-970, Belo Horizonte, Brazil

Jörg Schulze and Ignaz Eisele
Institut für Physik, Universität der Bundeswehr München, D-85577 Neubiberg, Germany

(Received 24 March 1999; accepted for publication 10 August 1999)

We develop the theory for grazing incidence small-angle x-ray scattering (GISAXS) from nanometer-sized naked islands on a flat substrate in the framework of the distorted-wave Born approximation (DWBA). The scattered wave amplitude is composed of four terms, including all combinations of scattering from the islands and reflection from the substrate. We apply this theory to x-ray measurements on Ge islands grown on Si(111), and show that we can determine the full triangular symmetry of these islands. The results also show that the DWBA must be used for smooth substrates near the angle of total external reflection. We finally discuss the advantages of GISAXS as compared to transmission small angle x-ray scattering for determining the symmetry of nanostructures. © *1999 American Institute of Physics.* [S0021-8979(99)02022-8]

I. INTRODUCTION

The self-assembled growth of nanometer-sized islands has recently become a strong field of research, mostly due to the possibility of obtaining well-defined nanostructures with new optoelectronic properties.[1] These islands are usually obtained by heteroepitaxial growth, with a small difference in lattice parameter between the substrate and the material being deposited. The resulting strain at the substrate/film interface eventually leads to the formation of self-assembled islands, in the well-known Stranski-Krastanow mode of growth.[2]

Morphological characterization of these islands is usually done using scanning probe microscopy techniques or x-ray scattering. The latter has advantages, e.g., there are no tip artifacts, it can be used even for buried islands, and the whole sample surface is analyzed leading to much better statistics for averaged values. X-ray scattering has been used to determine both the size and shape of these islands using grazing incidence small angle x-ray scattering (GISAXS).[3,4] In addition, x-rays can reveal the inner crystalline structure of the islands, their orientation and strain state when used in either grazing incidence diffraction[5] or crystal truncation rod (CTR) x-ray scattering.[6,7] Amorphous oxide layers covering the island, for example, can also be separated from a crystalline core. Especially from analyzing CTRs, facet angles can be determined with much higher precision than in scanning probe microscopy. However, the interpretation of scattering data is less direct than that of real space images and needs an appropriate theory.

In the past, GISAXS data have been analyzed in the framework of the Born approximation (BA) in order to determine the structure of these small islands.[8] We present here the scattering cross section calculated in the distorted-wave Born approximation (DWBA). In the application of this theory to GISAXS of triangular Ge islands on a Si(111) surface, we show that the DWBA has to be used in case one is working near the angle of total external reflection on very smooth surfaces, i.e., when the substrate reflectivity is high.

This article is organized as follows. In Sec. II we discuss the theory of small angle x-ray scattering from nanostructures on a flat substrate under grazing incidence conditions in the framework of the DWBA. We show that the scattering cross section can be considerably different from the Born approximation, which is also retrieved in the limiting case of vanishing substrate reflectivity. In Sec. III we apply our theory to Ge islands on boron-terminated Si(111), previously analyzed by atomic force microscopy (AFM). Shape, symmetry and orientation are determined by fitting the DWBA structure factor of pyramidal islands to the x-ray data. In Sec. IV we discuss the advantage of GISAXS as compared to SAXS for the analysis of symmetry properties. Finally in Sec. V we present our conclusions.

The geometry of GISAXS is shown in Fig. 1. The sample is positioned in an angle α_i with respect to the incoming x-ray beam. In our experiments, the scattering from the islands near the forward direction is collected by a one-dimensional position sensitive detector parallel to the surface

[a]Electronic mail: rauscher@stat.physik.uni-muenchen.de
[b]Also with Universidade Federal de Minas Gerais.

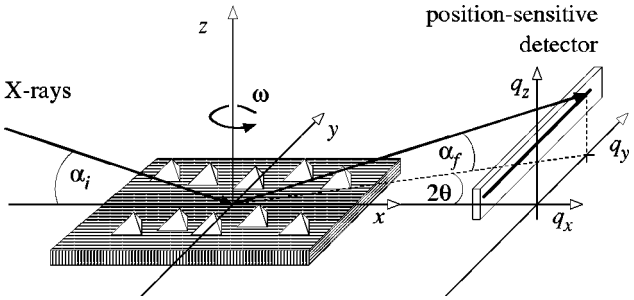

FIG. 1. Scattering geometry of grazing incidence small angle x-ray scattering used to study nanostructures deposited on a substrate. The incident beam impinges on the surface at an angle α_i and the scattered intensity is measured as a function of the exit angle α_f with respect to the substrate and 2θ with respect to the plane of incidence. The angles are mapped to the momentum transfer $\mathbf{q}=(q_x,q_y,q_z)$.

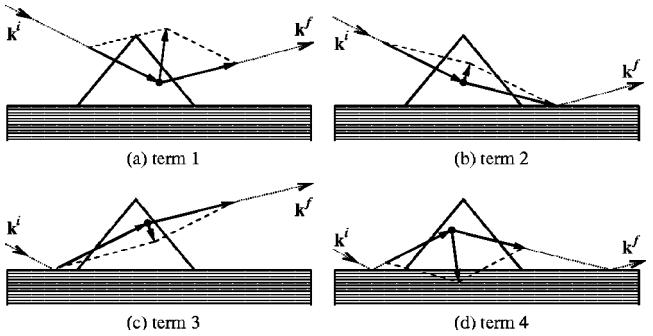

FIG. 2. The four terms of the scattered amplitude according to Eq. (10). (a) The incoming beam is scattered in the island and goes directly to the detector. This term is the scattered amplitude in the Born approximation. (b) The scattered beam is reflected by the surface and goes then to the detector. (c) The incoming beam is reflected before it is scattered. (d) The incoming and the scattered beam are reflected. Although the reflection of x-rays may occur inside the islands, as in (c), for example, in the DWBA R^i and R^f are the vacuum/substrate reflectivities. The arrows inside the islands indicate the net momentum transfer.

at an exit angle α_f. In this way, we measure the small angle scattering in 2θ scans for different angles ω, α_i and α_f.

II. THEORY OF GRAZING INCIDENCE SMALL ANGLE X-RAY SCATTERING

In order to calculate the scattered intensity from islands deposited on a substrate, either in the BA or the DWBA, we consider the sample substrate as a semi-infinite and homogeneous medium extending over the lower half space $z<0$. We describe the incident beam by the wave vector $\mathbf{k}^i=k_0(\cos\alpha_i,0,-\sin\alpha_i)$ with modulus k_0, corresponding to the vacuum wavelength $\lambda=2\pi/k_0$, and the scattered wave by $\mathbf{k}^f=k_0(\cos 2\theta\cos\alpha_f,\sin 2\theta\cos\alpha_f,\sin\alpha_f)$ of equal modulus, see Fig. 1. The scattering vector is denoted by

$$\mathbf{q}=\mathbf{k}^f-\mathbf{k}^i=k_0\begin{pmatrix}\cos 2\theta\cos\alpha_f-\cos\alpha_i\\ \sin 2\theta\cos\alpha_f\\ \sin\alpha_f+\sin\alpha_i\end{pmatrix}. \tag{1}$$

For small scattering angles the atomistic structure of the medium can be ignored and since the index of refraction is approximately one for hard x-rays, i.e., $n-1=\mathcal{O}(10^{-6})$, polarization effects are negligible, too.

In this approximation, the amplitude of the electromagnetic field $\Psi(\mathbf{r})$, i.e., either the electric or magnetic component, satisfies the stationary wave equation

$$[\nabla^2+n^2(\mathbf{r})k_0^2]\Psi(\mathbf{r})=0 \tag{2}$$

with the index of refraction $n^2(\mathbf{r})=n_0^2(z)+(1-n_\Delta^2)\chi_\Delta(\mathbf{r})$. The substrate is described by $n_0(z)$, i.e., $n_0(z)$ is one for $z>0$ and the index of refraction of the substrate n_s for $z<0$, respectively. The term n_Δ is the index of refraction of the islands and the characteristic step function $\chi_\Delta(\mathbf{r})$ is 1 inside and 0 outside the islands. For the bare substrate, i.e., for $\chi_\Delta(\mathbf{r})=0$, the wave Eq. (2) is solved by the Fresnel function

$$\Psi^0(\mathbf{r},\mathbf{k})=e^{i\mathbf{k}_\parallel\cdot\mathbf{r}_\parallel}\begin{cases}e^{ik_zz}+R_Fe^{-ik_zz}, & \text{if } z>0\\ T_Fe^{i\tilde{k}_zz}, & \text{if } z<0\end{cases} \tag{3}$$

with $\mathbf{r}_\parallel=(x,y)$, for an incoming plane wave with wave vector $\mathbf{k}=(\mathbf{k}_\parallel,k_z)$ and $k_z=-\sqrt{k_0^2-|\mathbf{k}_\parallel|^2}$. The vertical component of the wave vector in the substrate is $\tilde{k}_z=-\sqrt{n_s^2k_0^2-|\mathbf{k}_\parallel|^2}$ and the Fresnel reflectivity R_F and transmittivity T_F are given by

$$T_F=\frac{2k_z}{k_z+\tilde{k}_z}\quad\text{and}\quad R_F=\frac{k_z-\tilde{k}_z}{k_z+\tilde{k}_z}. \tag{4}$$

For interfaces with a finite width $\sigma>0$, the reflectivity and transmittivity are modified according to[9]

$$R=R_F\,e^{-2\sigma^2k_z\tilde{k}_z}\quad\text{and}\quad T=T_Fe^{-1/2\sigma^2(\tilde{k}_z-k_z)^2}. \tag{5}$$

These formulas hold for microscopically rough interfaces with rms roughness σ, too, as long as the correlation length is much smaller than $2\pi/|\mathbf{q}_\parallel|$, where $\mathbf{q}_\parallel=(q_x,q_y)$ is the component of the momentum transfer $\mathbf{q}$ parallel to the surface.

Now, we treat the islands as a perturbation and obtain in first order[10] the scattered amplitude

$$\Psi^{sc}(\mathbf{r})=-k_0^2(1-n_\Delta^2)\frac{e^{ik_0r}}{4\pi r}\times\int d^3r'\Psi^0(\mathbf{r}',-\mathbf{k}^f)\chi_\Delta(\mathbf{r}')\Psi^0(\mathbf{r}',\mathbf{k}^i). \tag{6}$$

Since the islands are located on top of the surface, $\Psi^0(\mathbf{r},-\mathbf{k}^f)$ and $\Psi^0(\mathbf{r},\mathbf{k}^i)$ are given by the expression for $z>0$ in Eq. (3) and thus both consist of two plane waves, an incoming and a reflected part. The scattered amplitude is therefore a sum of four Fourier integral transforms[11]

$$\tilde{\chi}_\Delta(\mathbf{q}_\parallel,\pm k_z^i\pm k_z^f)=\int d^3r e^{-i\mathbf{q}_\parallel\cdot\mathbf{r}_\parallel-i(\pm k_z^i\pm k_z^f)z}\chi_\Delta(\mathbf{r}) \tag{7}$$

with each of the four combinations of signs corresponding to one of the four combinations of incoming and exiting beams, as illustrated in Fig. 2. Written in terms of the Fourier transform of the characteristic function of the islands $\tilde{\chi}_\Delta(\mathbf{q}_\parallel,q_\perp)$, i.e., the shape factor, the scattered amplitude is given by

$$\Psi^{sc}(\mathbf{r}) = -k_0^2(1-n_\Delta^2)\frac{e^{ik_0 r}}{4\pi r}[\tilde{\chi}_\Delta(\mathbf{q}_\parallel, q_z) + R^f\tilde{\chi}_\Delta(\mathbf{q}_\parallel, -p_z) + R^i\tilde{\chi}_\Delta(\mathbf{q}_\parallel, p_z) + R^iR^f\tilde{\chi}_\Delta(\mathbf{q}_\parallel, -q_z)] \quad (8)$$

with $p_z = k_z^f + k_z^i$, where $q_\perp$ corresponds to the net momentum transfer perpendicular to the substrate surface. The reflectivities for the incoming and outgoing waves are denoted R^i and R^f, respectively. Here we point out that the value of p_z can be considerably smaller than q_z, e.g., $p_z = 0$ for $\alpha_i = \alpha_f$ since then $k_z^i = -k_z^f$.

Each term is related to one of the scattering processes illustrated in Fig. 2. The first term consists of a single x-ray scattering event in an island. The second term reflects the possibility of scattering by an island and subsequent reflection from the substrate. In the third term the reflection by the substrate occurs first, and then the x-rays are scattered by an island. Finally the fourth term is related to a double reflection by the substrate, with the scattering at an island in between. The three latter shape factor terms are accordingly multiplied by different substrate reflectivity coefficients, since each time the x-rays are reflected by the substrate they are attenuated depending on the incident angle. The arguments in the shape factors of the four terms are the net momentum transfers, considering all scattering and reflection processes.

We emphasize here that the scattered amplitude Ψ^{sc} in Eq. (8) is not only a function of the momentum transfer $\mathbf{q}$, either in the vacuum or in the substrate, but depends explicitly on k_z^i and k_z^f. Since the islands are on top of the surface, q_z and p_z are real and the substrate's index of refraction enters in the formula only in the reflectivities, in contrast to the theory of diffuse scattering of buried structures.[10] There, the amplitude is mediated by the transmission function rather than the reflectivity.

The diffuse differential cross section is then given by

$$\frac{d\sigma}{d\Omega} = r^2|\Psi^{sc}(\mathbf{r})|^2 = \frac{k_0^4|1-n_\Delta^2|^2}{(4\pi)^2}S(\mathbf{q}_\parallel, k_z^f, k_z^i), \quad (9)$$

with the structure factor

$$S(\mathbf{q}_\parallel, k_z^f, k_z^i) = |\tilde{\chi}_\Delta(\mathbf{q}_\parallel, q_z) + R^f\tilde{\chi}_\Delta(\mathbf{q}_\parallel, -p_z) + R^i\tilde{\chi}_\Delta(\mathbf{q}_\parallel, p_z) + R^iR^f\tilde{\chi}_\Delta(\mathbf{q}_\parallel, -q_z)|^2. \quad (10)$$

The structure factor in the Born approximation is given by the same equation only with $R^{i,f} = 0$, i.e., by the absolute square of the first term. This means that the BA is valid when the Fresnel reflectivities are small, either because the incident and exit angles are much larger than the angle of total external reflection or the substrate surface is very rough. In this case the three latter terms in Eq. (10), which are multiplied by substrate reflectivity coefficients, are negligible and the first term becomes dominant.

III. GISAXS FROM NAKED TRIANGULAR Ge ISLANDS

We applied our theory to x-ray scattering from Ge islands on Si(111) prepared by molecular beam epitaxy in an ultrahigh vacuum (UHV) system.[12] The substrate (kept at 530 °C) was a Si(111) wafer, on which a 1500 Å Si buffer layer was grown, followed by 1/3 monolayer of boron. Subsequently a 150-Å-thick Ge layer was deposited at a rate of 0.25 Å/s yielding triangular pyramidal islands.[13]

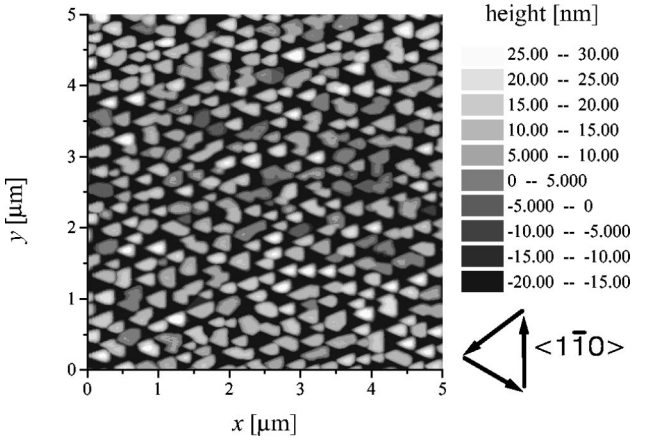

FIG. 3. Two-dimensional plot of an atomic force microscopy measurement of Ge islands on boron-terminated Si(111). Most islands exhibit a triangular pyramidal shape oriented in the $\langle 1\bar{1}0\rangle$ direction (see arrows). This full orientation of the islands allows us to determine their symmetry using GISAXS.

The morphology of this sample was analyzed with an atomic force microscope, as can be seen in Fig. 3. The substrate surface is filled with triangular pyramids with well-defined {113} facets,[14] with a base side $L \approx 2500$ Å and a height $H = 300-500$ Å. Some of the islands exhibit a small (111) terrace on top. There is an obvious unidirectional orientation of the islands, probably induced by the substrate terraces. This orientation is essential to determine the island symmetry in a scattering experiment. In our sample the substrate miscut was approximately 0.14° off the $\langle 111\rangle$ direction. The substrate terrace ledges cut the x axis in Fig. 3 at an angle of $7° \pm 5°$ with ledges running from the upper left to the lower right and steps facing upwards.

The GISAXS measurements were performed at the surface x-ray beamline ID-3 at the European Synchrotron Radiation Facility (ESRF) in Grenoble, France. The sample surface was illuminated at a grazing angle α_i with a highly collimated x-ray beam of wavelength $\lambda = 1.22$ Å. The scattering angle α_f was set to a different value than α_i to collect only diffuse intensity, as in Ref. 15. The diffuse x-ray scattering from the islands was measured with a position-sensitive detector aligned parallel to the sample surface as a function of q_y.

In Fig. 4 we show the x-ray data taken for several azimuthal angles ω but with constant $\alpha_i = 0.44°$ and $\alpha_f = 0.7°$, i.e., $q_z = 0.102\,\text{Å}^{-1}$ and $p_z = 0.023\,\text{Å}^{-1}$. We show selected scans in this geometry, where the symmetry properties of the patterns change with ω. The direction $\omega = 0°$ corresponds to the $\langle 1\bar{1}0\rangle$ direction being parallel to the incident beam, see Fig. 3. At $\omega = -30°$ the scattering pattern is symmetrical. For $\omega = 0°$ the scattered intensity from the islands exhibits

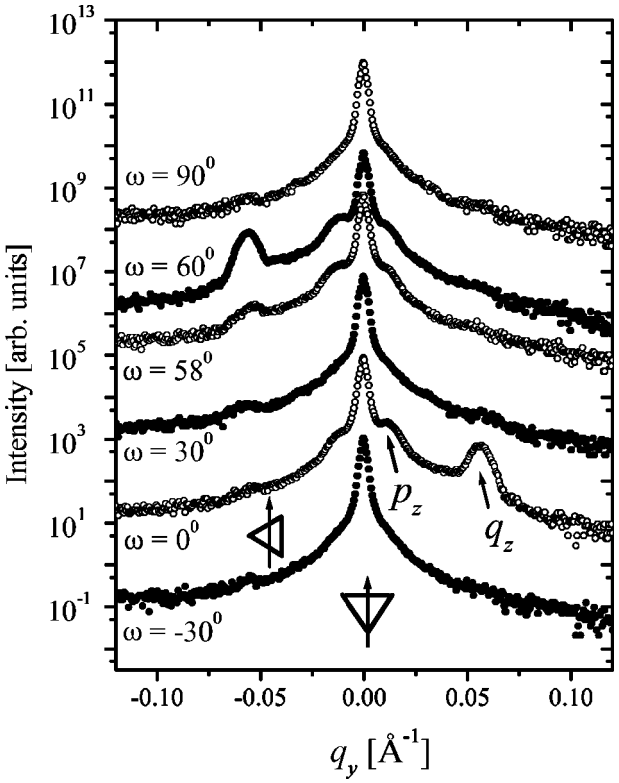

FIG. 4. GISAXS from our Ge triangular islands and several ω angles. Note the outer and inner shoulders on the right of the central peak for the $\omega = 0°$ scan, corresponding to the {113} CTR for q_z and p_z, respectively (their positions are indicated by arrows). The triangles indicate the orientation of the islands with respect to the incoming beam (arrow).

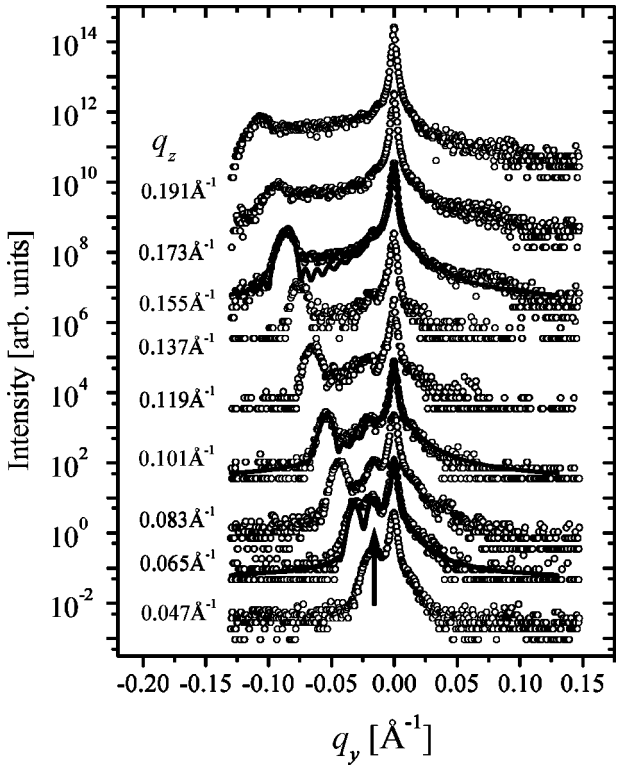

FIG. 5. Scans in GISAXS geometry varying α_i and α_f with constant p_z. The peak moving to the left for increasing q_z corresponds to the direct {113} CTR, whereas the smaller shoulder, i.e., the reflected CTR (see arrow), tends to disappear due to the decrease of R^i for large incident and exit angles.

two shoulders on the right side of the central peak where the strongest corresponds to the {113} crystal truncation rod (CTR, due to the faces of the pyramid) for $q_\perp = q_z = 0.102\,\text{Å}^{-1}$, where $q_\perp$ is the momentum transfer perpendicular to the surface. The smaller shoulder near the central peak corresponds to the same CTR reflected once by the substrate surface, i.e., stemming from a smaller momentum transfer $q_\perp = p_z = 0.023\,\text{Å}^{-1}$. These shoulders move to the left after the sample has been turned to $\omega = 60°$, and return to their original position for $\omega = 120°$ (not shown here). The patterns are symmetrical when $\omega = -30°$, 30°, 90°, 150°, etc. The symmetry properties of these patterns indicate the triangular symmetry of the islands and their unidirectional orientation.

For the fits of the scattering profiles we neglect possible correlations in the positions of the islands since these cannot be resolved in our 2θ scans. Thus, the scattered intensity is essentially a function of the Fourier transform of a single island. Because of the triangular symmetry and the {113} CTR, we assume a triangular pyramidal shape for the islands, which is consistent with the AFM measurements. As indicated by the AFM, we include a top terrace in our numerical Fourier transformation of the pyramid's characteristic step function. The Fourier transform of an equal sided triangle with side length a is known analytically

$$\tilde{\chi}_{\text{tri}}(q_x, q_y, a) = \frac{\sqrt{6} e^{-i\sqrt{3} q_y a/6}}{q_x (q_x^2 - 3q_y^2)} \times \left(q_x e^{i\sqrt{3} q_y a/2} - q_x \cos\left(\frac{q_x a}{2}\right) - i\sqrt{3} q_y \sin\left(\frac{q_x a}{2}\right)\right). \tag{11}$$

Only the integration over triangular sections with linearly decreasing sides $a(z) = (1 - z/h) L_{\text{bot}}$ in the z direction remains for numerical integration

$$\tilde{\chi}_\Delta(q_x, q_y, q_z) = \int_0^{h(1 - L_{\text{top}}/L_{\text{bot}})} dz \tilde{\chi}_{\text{tri}}(q_x, q_y, a(z)) e^{i q_z z}, \tag{12}$$

where L_{bot} and L_{top} correspond to the bottom and top triangle sides and H is the height of the pyramid.

The importance of the use of the DWBA can be seen in Fig. 5 as we increase the values of α_i and α_f at the same time. These scans were performed with a constant offset between α_i and α_f of 0.36° corresponding to a constant value for $p_z = 0.032\,\text{Å}^{-1}$. As we varied α_i from 0.1° to 0.9°, q_z ranged from $0.047\,\text{Å}^{-1}$ to $0.191\,\text{Å}^{-1}$. We can clearly observe the smaller second shoulder near the central peak vanishing as α_i is increased. This is a result of the decrease of the substrate reflectivity. The small shoulder also does not move since our scans were performed with fixed p_z. At the

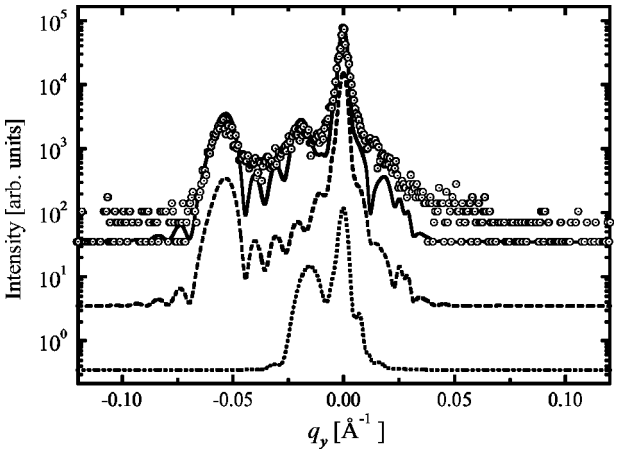

FIG. 6. Comparison of the GISAXS pattern from our islands to the components of the DWBA. The circles represent a 2θ scan from the triangular Ge islands with $\alpha_i = 0.385°$, $\alpha_f = 0.74°$ and $\omega = 60°$. The dashed line corresponds to the first term of Eq. (10) which is also the BA for $q_z = 0.101\,\text{Å}^{-1}$. The dotted line is the third term, with $p_z = 0.032\,\text{Å}^{-1}$. The solid line is the sum of all four terms. The curves are offset by one order of magnitude for clarity.

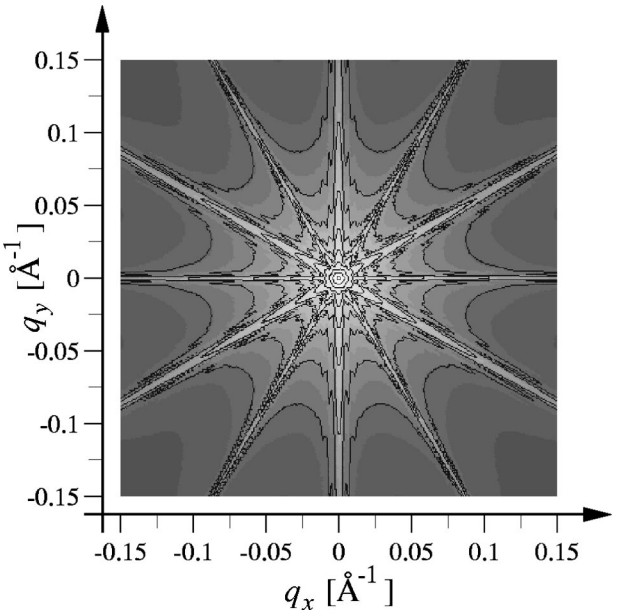

FIG. 7. The q_x-q_y mapping of the structure factor of our triangular islands in BA for $q_z = 0$ yielding a sixfold pattern.

same time the q_z-{113} CTR moves outwards and is still clearly visible at much higher values of α_i and α_f.

Least-square fits of three selected patterns of Fig. 5 were performed simultaneously,[16] yielding $H = (430 \pm 30)$ Å, $L_{\text{bot}} = (2800 \pm 200)$ Å, $L_{\text{top}} = (530 \pm 100)$ Å and a Gaussian size distribution with full width at half maximum (FWHM) $= 10\%$. The fits also included a small diffuse scattering Lorentzian term (FWHM$= 0.015\,\text{Å}^{-1}$) induced by the buffer roughness and a number of structures that have coalesced.[13]

In Fig. 6 we show a comparison of the data for $q_z = 0.101\,\text{Å}^{-1}$ ($\alpha_i = 0.385°$, $\alpha_f = 0.74°$, and $p_z = 0.032\,\text{Å}^{-1}$) to the separate contributions from the first and third terms of Eq. (10), together with the total calculated scattered intensity. We used the fitted parameters for the islands obtained in Fig. 5, without the size distribution. The second and fourth terms are negligible because $R^f(0.74°) = -0.028 + 5.94 \times 10^{-4} i$ is much smaller than $R^i(0.385°) = -0.123 + 3.19 \times 10^{-3} i$. It can be clearly observed that the dotted line, corresponding to the third term, is similar to the dashed line which represents the first term, i.e., the BA. However, since the value of the momentum transfer component perpendicular to the substrate $p_z = 0.032\,\text{Å}^{-1}$ is considerably smaller than $q_z = 0.101\,\text{Å}^{-1}$, we obtain a pattern shrunk by a factor of $p_z/q_z = 0.32$.

IV. SYMMETRY IN SAXS AND GISAXS

As can be seen above, we were able to determine the symmetry and orientation of the triangular islands using GISAXS. In a conventional small angle scattering setup, this could not be accomplished, since there is no momentum transfer component perpendicular to the surface, i.e., $q_z = 0$. To understand this, we present here the discussion of the differential cross section in the BA, which is given by the first term of Eq. (10). This discussion can be extended to the DWBA by including the three other terms in the structure factor.

Since the scattered amplitude is proportional to the Fourier transform of the islands' shape [see Eq. (8)], it represents their symmetry perfectly. However, in x-ray scattering experiments, only the absolute square of the scattered amplitude is accessible, i.e., $S(\mathbf{q})$. The information about the phase of the scattered wave is lost. In particular, the structure factor and thus the scattered intensity is the same for $\mathbf{q}$ and $-\mathbf{q}$, i.e., $S(\mathbf{q}) = S(-\mathbf{q})$. In the case of a transmission geometry experiment the momentum transfer component parallel to the incoming beam vanishes, i.e., $q_z = 0$. This means that the scattered signal is the same, when the sample is turned by 180° around the direction of the incoming beam, even if the islands do not have any even rotational symmetry. Thus, such an experiment cannot distinguish between threefold and sixfold symmetries, for example. This corresponds to Friedel's law in x-ray diffraction,[17] which says that the inversion of a crystal through a center of symmetry does not change the diffraction intensity in the kinematical approximation. As an example we show in Fig. 7 a q_x-q_y mapping of the structure factor of our triangular islands as expected for a transmission geometry experiment with the incoming beam in the z axis. The sixfold symmetry is obvious.

The main reason for this phase problem is that the momentum transfer in the direction of the symmetry axis vanishes in transmission geometry. This is not the case in a grazing incidence experiment. There is a momentum transfer component in the direction perpendicular to the surface, i.e., $q_z \neq 0$, which at the same time is the threefold symmetry axis of our islands. A rotation of 180° around the z axis does not correspond to a change from $\mathbf{q}$ to $-\mathbf{q}$ and thus can change the structure factor, i.e., $S(q_x, q_y, q_z) \neq S(-q_x, -q_y, q_z)$. Only the rotation in combination with a reflection at the x-y plane gives us the same structure factor. A q_x-q_y mapping of the pyramid structure factor for $q_z > 0$ is shown in Fig. 8. The threefold symmetry of the islands clearly appears.

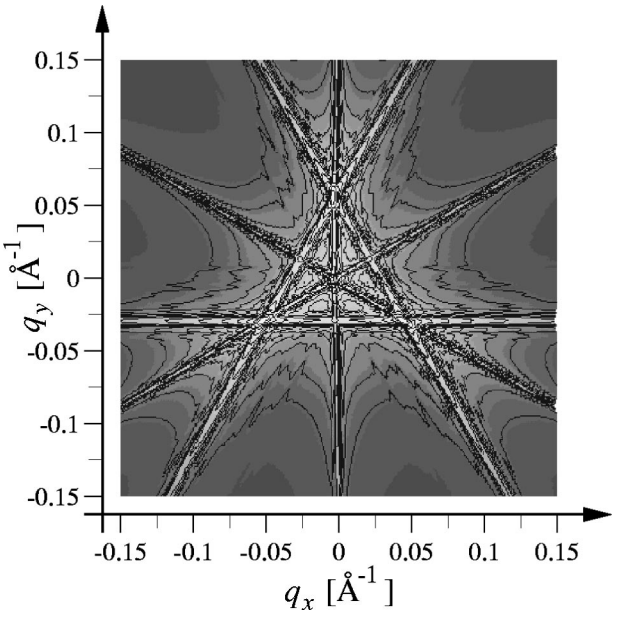

FIG. 8. The q_x-q_y mapping of the structure factor of the triangular islands in BA for $q_z = 0.101$ Å^{-1}. The edges of the central triangle correspond to the {113} CTRs of the side facets.

However, it is not possible to determine the complete symmetry of *any* nanostructure. For example, a triangular prism with the symmetry axis perpendicular to the surface would have a structure factor with a sixfold symmetry. It has an additional up-down symmetry and its shape does not change when mirrored with respect to the x-y plane. All three CTRs of the side faces lie in the x-y plane and form a sixfold star. The three CTRs of the pyramid's side facets do not lie in the x-y plane and form a three-dimensional pattern with threefold symmetry. Therefore the complete symmetry of a structure cannot be determined if it has an up-down symmetry.

In the DWBA the mappings become more complicated as they are the sum of four shape factors for different momentum transfer components $\pm q_z$ and $\pm p_z$ and multiplied by different reflection coefficients. However, the same arguments given above still hold and the structure factor is threefold, as long as at least one of the angles of incidence or exit is larger than the angle of total external reflection α_c. If both α_i and α_f are smaller or equal than α_c, the reflectivities $R^i = R^f = 1$ (neglecting the substrate absorption) and all four terms are equally weighted. In this case the first and the last, as well as the second and third terms, add up to a sixfold pattern again due to their inversion symmetry. We illustrate this in Fig. 9, where we plot the GISAXS q_y-q_z mapping with $\alpha_i = \alpha_c$ and α_f varying from 0° to 1°. In this plot both q_z and p_z vary since $\alpha_f - \alpha_i$ is not constant as in Fig. 5. For $\alpha_f > \alpha_c$ the direct and reflected {113} CTR is visible on the left, whereas for $\alpha_f < \alpha_c$ we observe a pattern symmetric with respect to the q_z axis.

V. CONCLUSIONS

In summary we developed a scattering theory for nanostructures on top of flat surfaces based on the distorted-wave Born approximation. The scattered amplitude is composed of four contributions, including all combinations of scattering from the islands and reflection from the substrate surface. We applied our theory to GISAXS at self-assembled Ge islands on a Si(111) surface and compared our results with AFM measurements. The scattered intensity of the islands was fitted assuming a triangular pyramidal shape with a small (111) top facet and {113} side facets, in agreement with the AFM results. We showed, that the DWBA has to be used when the surface reflectivity for the incoming or the outgoing beam is high, i.e., near or below the angle of total external reflection. Thus shape, size and complete symmetry of the islands could be determined from the x-ray data. A discussion of the differences between the conventional SAXS geometry and GISAXS proves that the small angle analogy to the Friedel law can be circumvented for oriented structures in grazing incidence geometry.

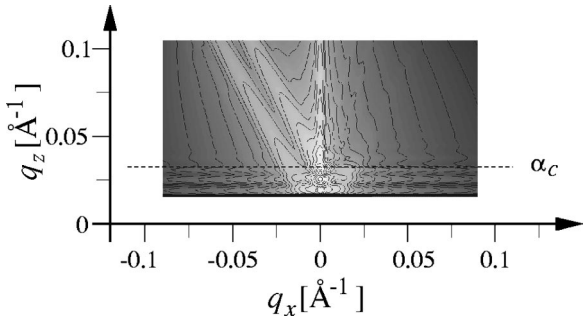

FIG. 9. Mapping of the small angle x-ray scattered intensity in the q_y-q_z plane for constant $\alpha_i = \alpha_c = 0.177°$. For $\alpha_f > \alpha_c$ the {113} CTR (for both direct and reflected beams) is visible on the left, whereas for $\alpha_f < \alpha_c$ we observe a pattern symmetric with respect to the q_z axis.

ACKNOWLEDGMENTS

This research was supported by the Volkswagen Stiftung unter Contract No. I/72512, by the PROBRAL exchange program (DAAD/CAPES) and by ESRF. M. Rauscher acknowledges support by the DFG. R. Paniago thanks CNPq for financial support. The authors thank Salvador Ferrer for support at the ID3-ESRF beamline.

[1] For a review, see, e.g., Mater. Res. Soc. Bull. **23** (1998).
[2] I. N. Stranski and L. Von Krastanow, Akad. Wiss. Lit. Mainz Abh. Math. Naturwiss. Kl. **146**, 797 (1939).
[3] M. Schmidbauer, Th. Wiebach, H. Raidt, R. Köhler, and H. Wawra, Phys. Rev. B **58**, 10523 (1998).
[4] J. R. Levine, J. B. Cohen, Y. W. Chung, and P. Georgopoulos, J. Appl. Crystallogr. **22**, 528 (1989).
[5] I. Kegel, T. H. Metzger, P. Fratzl, J. Peisl, A. Lorke, J. M. Garcia, and P. M. Pettroff, Europhys. Lett. **45**, 222 (1999).
[6] A. J. Steinfort, P. M. L. O. Scholte, A. Ettema, F. Tuinstra, M. Nielsen, E. Landemark, D.-M. Smilgies, R. Feidenhans'l, G. Falkenberg, L. Seehofer, and R. L. Johnson, Phys. Rev. Lett. **77**, 2009 (1996).
[7] F. B. Rasmussen, J. Baker, M. Nielsen, R. Feidenhans'l, and R. L. Johnson, Phys. Rev. Lett. **79**, 4413 (1997).
[8] See, e.g., H. You, K. G. Huang, and R. T. Kampwirth, Physica B **221**, 77 (1996).
[9] L. Nevot and P. Croce, Phys. Rev. Appl. **15**, 761 (1980).

[10] M. Rauscher, T. Salditt, and H. Spohn, Phys. Rev. B **52**, 16855 (1995).
[11] For rough interfaces, we neglect the finite width of the interface in the integration, since our analysis is only valid for σ much smaller than the islands' height.
[12] A. V. Zotov, M. A. Kulakov, S. V. Ryzhkov, V. G. Lifshits, B. Bullemer, and I. Eisele, Surf. Sci. **352–354**, 358 (1996).
[13] R. Paniago, H. Metzger, M. Rauscher, J. Peisl, J. Schulze, I. Eisele, and S. Ferrer, J. Appl. Crystallogr. (submitted).
[14] U. Köhler, O. Jusko, G. Pietsch, B. Müller, and M. Henzler, Surf. Sci. **248**, 1321 (1991).
[15] R. Paniago, R. Forrest, P. C. Chow, S. C. Moss, S. S. P. Parkin, and D. Cookson, Phys. Rev. B **56**, 13442 (1997).
[16] As the observed reflectivity was larger than expected for a pure silicon substrate, we used the index of refraction of Ge in the calculation of the substrate reflectivities. The presence of a Ge wetting layer on Si is common in this Stranski-Krastanow type of growth.
[17] J. M. Cowley, *Diffraction Physics* (North-Holland, Amsterdam, 1975).